

# Low Temperature, Rapid Thermal Cycle Annealing of HgCdTe Grown on CdTe/Si

SINA SIMINGALAM,<sup>1,2,3,4</sup> GREGORY BRILL,<sup>2,5</sup>  
PRIYALAL WIJEWARNASURIYA,<sup>2,6</sup> and MULPURI V. RAO<sup>3,7</sup>

1.—School of Physics, Astronomy and Computational Sciences, George Mason University, Fairfax, USA. 2.—US Army Research Laboratory, Adelphi, USA. 3.—Department of Electrical and Computer Engineering, George Mason University, Fairfax, USA. 4.—e-mail: ssuminga@gmu.edu. 5.—e-mail: gregory.n.brill.civ@mail.mil. 6.—e-mail: priyalal.wijewarnasuriya@us.army.mil. 7.—e-mail: rmulpuri@gmu.edu

The HgCdTe(MCT) grown on CdTe/Si substrate has a high dislocation density due to lattice mismatch. Thermal cycle annealing (TCA) is effective in reducing the dislocation density. The TCA at high temperatures results in inter-diffusion of the constituent elements across the MCT/CdTe interface. In this study, we observed a reduction in dislocation density with good surface morphology due to proper design of the TCA system, low annealing temperature, and large number of annealing cycles. The ampoule containing the samples is placed in direct contact with the graphite heating tube which helps in increasing the heating and cooling rates of the annealing cycle. To maintain Hg overpressure, Hg is placed in the sample holder, instead of in the ampoule to avoid Hg condensation. The best results were obtained by cycling the annealing temperature between 290°C and 350°C. Anneals were performed by using 32, 64, 128 and 256 cycles. We obtained an etch pit density (EPD) as low as  $1 \times 10^6 \text{ cm}^{-2}$ . Lower EPD was not achieved either by increasing annealing temperature or number of annealing cycles. Through secondary ion mass spectroscopy analysis, we observed very little inter-diffusion of Cd across the MCT/CdTe interface for the 128 cycle annealing. These results show promise in bridging the gap in the device performance between the MCT material grown on CdTe/Si and CdZnTe substrates.

**Key words:** HgCdTe, thermal cycle annealing, dislocation, diffusion

## INTRODUCTION

HgCdTe (MCT) is the material of choice for infrared sensor applications since its discovery in the 1950s.<sup>1</sup> Optimal molecular beam epitaxy (MBE) growth of MCT has been achieved on (211)B oriented surfaces and the preferred substrate is lattice-matched, bulk CdZnTe. Its high cost of more than \$200  $\text{cm}^{-2}$  and limited size of  $7 \times 7 \text{ cm}^2$  have created a push to obtain alternative substrates with similar performance.<sup>2,3</sup> Several alternative substrates have been researched over the past two decades.<sup>4-6</sup> The current alternative substrate of choice is silicon due to its cost of less than \$1  $\text{cm}^{-2}$

and large format size of greater than 8" in diameter.<sup>7,8</sup> It also has the added benefit of being thermally matched to the silicon read-out integrated circuit. The issue to overcome with using silicon based substrates is the ~19% lattice mismatch with the MCT layer. Typically, a thin layer of ZnTe and several microns of CdTe are grown on top of the silicon prior to the growth of MCT to bridge the lattice mismatch.<sup>9</sup> The substrate defect density of the CdTe is in the mid- to low- $10^5 \text{ cm}^{-2}$  range. This is an order of magnitude higher than the dislocation density in bulk CdZnTe substrates and leads to a higher dislocation density in the final MCT absorber layer grown on CdTe/Si.<sup>10</sup>

Dislocation density is a problem due to shunt current paths formed along the dislocations through

(Received August 16, 2014; accepted November 17, 2014; published online December 12, 2014)

the  $p$ - $n$  junction of the MCT diodes, lowering the device performance.<sup>11</sup> High temperature thermal cycle annealing (TCA) has been shown to reduce the dislocation density in MCT grown on CdTe/Si substrates.<sup>12</sup> Application of this high-temperature TCA method to device fabrication is limited due to significant diffusion of Cd across the MCT/CdTe interface.

Structural integrity is necessary for optimal device performance. The main advantage of MBE is the ability to control the layer-by-layer structure and creation of sharp interfaces. If significant diffusion occurs during the post-growth annealing process, the advantage of using MBE for material growth is lost. Because of this, we looked at reducing the annealing temperature to minimize constituent diffusion.

The diffusion problem can be circumvented by decreasing the annealing temperatures and compensating the thermal budget by increasing the number of annealing cycles. The fast ramp-up and ramp-down of the annealing cycles also helps to decrease the diffusion of the constituent elements. In this study, we designed the annealing system to increase the ramp-up and ramp-down rates, and the maximum annealing temperature was kept at 350°C. The low temperature TCA in this study was tried on the MCT layers of different starting dislocation densities.

## MATERIALS AND METHODS

Samples of MCT were grown on  $2 \times 2 \text{ cm}^2$  CdTe/Si substrates by MBE in a DCA ultrahigh vacuum MBE growth chamber. The MCT was grown using a Hg background flux with CdTe, Te, and In sources with a substrate temperature of  $\sim 180^\circ\text{C}$ , as determined by a pyrometer. The growth rate was typically 1–2  $\mu\text{m/h}$ . Further details of MBE growth have been described elsewhere.<sup>4</sup> The MCT absorber layer composition was determined by post-growth Fourier-transform infrared (FTIR) spectroscopy using a Nicolet 8700 FTIR spectrometer. The as-grown MCT absorber layer has a typical x-ray diffraction (XRD) full-width at half-maximum (FWHM) of 100–200 arc-seconds and etch pit density (EPD) of around  $1 \times 10^7 \text{ cm}^{-2}$ . The typical device structure was grown with a cadmium-rich buffer layer of approximately 0.5  $\mu\text{m}$ , an absorber layer of 8–10  $\mu\text{m}$ , a cadmium rich cap layer of approximately 0.3  $\mu\text{m}$  and a  $\sim 30$ -nm CdTe cap layer. The Cd rich cap layer is used to minimize dark current by reducing the current generated in the  $p$ -type region of the diode.

Pieces ( $5 \times 5 \text{ mm}^2$ ) of the as-grown MCT were cleaved from the  $2 \times 2 \text{ cm}^2$  wafer and cleaned with solvents. The samples were then dipped for 10 s in a 10% HCl solution to remove any surface oxide and rinsed for 60 s under running de-ionized water. Samples were placed on a quartz sample holder inside a quartz ampoule, as shown in Fig. 1. Prior to loading of the samples, the quartz ampoule, plug

and sample holder were cleaned through a flameout procedure where they are placed under vacuum of  $10^{-6}$  Torr and heated with an oxygen–hydrogen torch to remove any contaminants. After the flameout, the ampoule, plug and sample holder were allowed to cool to room temperature. Once cool, 125  $\mu\text{L}$  of Hg was placed in a cavity of the sample holder intended for holding Hg away from samples. The quartz plug was placed  $\sim 10$  cm from the closed end of the ampoule. The ampoule was pumped down to low  $10^{-5}$  Torr vacuum and sealed around the quartz plug with the oxygen–hydrogen torch. To prevent heating of the samples during sealing, a wet cloth was wrapped around the ampoule near the position of the plug.

We conducted TCA by moving the ampoule between a high-temperature tube and a low-temperature tube. The TCA setup involves the use of graphite tubes placed in a furnace, as seen in Fig. 2. Graphite tubes have a high thermal mass allowing little variation in temperature through the length of the tube. The temperature inside the ampoule changes at a rate greater than  $100^\circ\text{C}$  per minute when the ampoule is moved from one temperature zone to the other zone, as seen in Fig. 3. After completing all cycles, the ampoule was moved into the low-temperature graphite tube and cooled to room temperature over several hours. This slow, controlled cooling process is necessary to prevent condensation of mercury on the surface and to prevent creation of Hg vacancies in the MCT material.

After cooling to room temperature, the samples were removed from the ampoule and etched for 30 s in 0.1% bromine–methanol 5  $\mu\text{m}$  from the surface, then rinsed twice in methanol and dried with dry nitrogen. To reveal the dislocations, the samples were etched with the Benson etch solution for 40 s, rinsed under running de-ionized water and dried.<sup>13</sup> The dislocations were observed under bright field microscopy using a Leica IN20 microscope and counted using computer software.

Before and after annealing, the MCT layer crystallinity was characterized using high-resolution XRD full-width, half-maximum (FWHM) measurements. This was accomplished through the use of an X'pert Pro Analytical system using a Cu- $K_\alpha$  source. The samples were characterized by  $\omega$ - $2\theta$  scans. Due to the  $4^\circ$  tilt of the sample, the XRD measurement was done at two different  $\omega$  angles and the FWHM was taken as an average between the two XRD FWHM measurements.

To look at the compositional integrity of the layers, secondary ion mass spectroscopy (SIMS) was used to determine the Cd composition throughout the material. SIMS was conducted using a Cs+ atom that strikes the surface with enough energy to eject the surface atom from the sample. We looked at the SIMS of the as-grown and annealed samples to determine the influence of annealing conditions on the compositional integrity of the grown material.



Fig. 1. Ampoule schematic showing samples, plug and mercury placement. Gray circle represents Hg. Green bars represent MCT samples. Design is not drawn to scale.

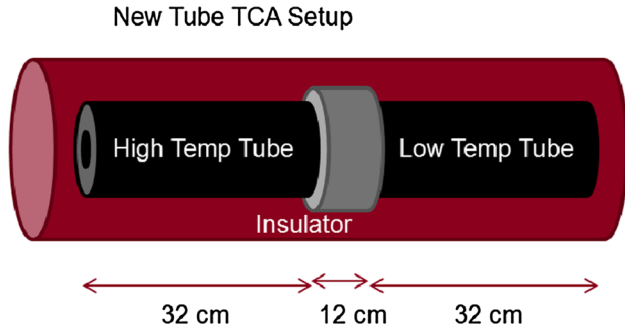


Fig. 2. Graphite tube setup. The tubes are centered in the furnace and heated to a preset temperatures.

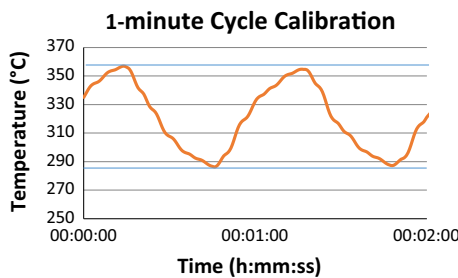


Fig. 3. The temperature inside the ampoule as it is cycled between the high-temperature and low-temperature tubes.

### RESULTS AND DISCUSSION

We started our work with 32 cycles of TCA at 450°C, 400°C, 370°C and 350°C. As shown in Fig. 4, we observed a significant reduction in EPD at temperatures as low as 350°C, but the EPD reduces exponentially with increasing temperature. The EPD seems to be approaching a minimum of  $1 \times 10^6 \text{ cm}^{-2}$  for 32 cycle annealing at 450°C. Previously published data have shown that the dislocation reduction is influenced more by increasing the number of cycles rather than extending the annealing time.<sup>14</sup> To examine the correlation between the number of cycles and the final EPD of the sample, we looked at the effect of 32, 64, 128, and 256 annealing cycles with the annealing temperatures held constant at 350°C and 290°C for several different samples. The dislocation density reduction is exponentially dependent on the number of cycles and again saturates near  $1 \times 10^6 \text{ cm}^{-2}$ , as seen in Fig. 5. To determine if this is an absolute limit, we conducted an experiment at an elevated annealing temperature of 400°C up to 512 anneal-

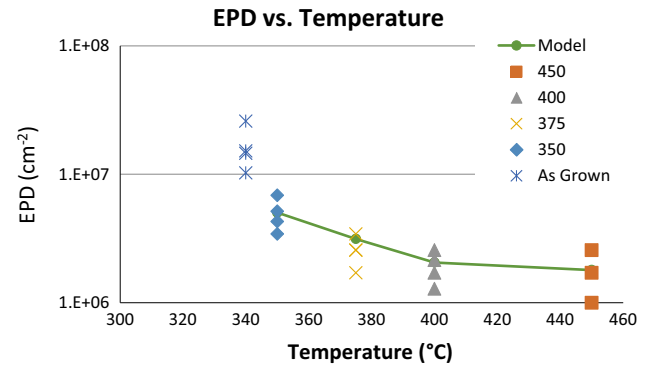


Fig. 4. Results of 32 cycle TCA on EPD of MCT grown on CdTe/Si substrates.

ing cycles, but were still unable to go below the EPD limit of  $1 \times 10^6 \text{ cm}^{-2}$ . This indicates a fundamental limitation to the use of silicon substrates for fabricating MCT planar devices. The  $1 \times 10^6 \text{ cm}^{-2}$  EPD is considered low enough for short-wavelength and mid-wavelength infrared device applications, but may not be attractive for the narrow band gap, long wavelength, infrared MCT detectors due to a high reverse bias dark current at this defect concentration.<sup>11</sup>

To correlate the data further, we characterized some of the annealed samples by XRD. The effect of TCA on crystallinity of the sample is seen in XRD measurements, as shown in Fig. 6. The pre-annealed, as-grown FWHM is 126'' and reduces to 85'' after being treated with the low-temperature (350°C), 128 cycle annealing. Final FWHM of TCA subjected samples ranges from 65'' to 90''. This value is similar to FWHM measurements by Farrell, et al.<sup>14</sup> who achieved minimum dislocation density of  $1 \times 10^6 \text{ cm}^{-2}$  after four 5-min, 494°C anneals with FWHM of 65''–80''. The total anneal time of the samples was about 2 h for both TCA schedules, but in the present study a significantly reduced annealing temperature was used to achieve similar material properties. An increased number of anneal cycles and faster heating and cooling rates in the present study are believed to be responsible for this result.

The theory for TCA causing dislocation reduction has been published previously.<sup>12</sup> Dislocation reduction at high anneal temperatures of 400°C, 450°C and 500°C have been modeled for MCT subjected to TCA.<sup>14</sup> Results of this work were analyzed using the model and corresponding values from

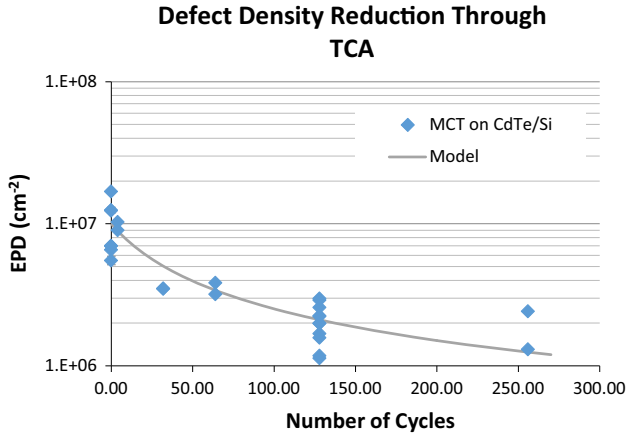


Fig. 5. EPD versus number of cycles between temperatures of 350°C and 290°C.

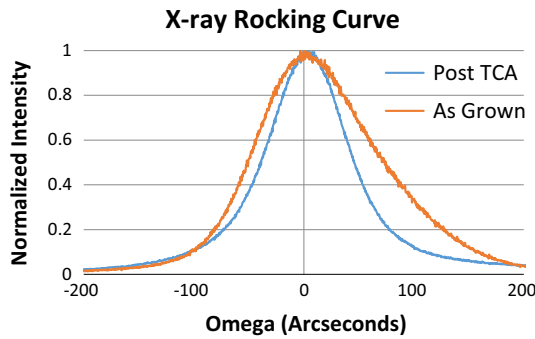


Fig. 6. X-ray omega-2theta measurements of an MCT sample grown on CdTe/Si as grown and post TCA. TCA characteristics include 350°C anneal temperature and 128 1-min cycles.

Benson et al. that describe dislocation interaction in MCT based on a previous dislocation model for GaAs grown on silicon substrates.<sup>15</sup> During annealing, dislocations interact through two main methods, coalescence and annihilation. Based on this model, the glissile and coalesced sessile dislocation densities,  $D_1$  and  $D_2$ , respectively, are given by

$$D_1 = \frac{D_0}{1 + D_0 k_2 t}$$

$$D_2 = 2nD_0^2 k_2 t$$

where  $D_0$  is the dislocation density at the start of the anneal cycle,  $n$  is the fraction of dislocations interacting through coalescence,  $t$  is the anneal time, and  $k_2$  is the coalescence reaction rate. The reaction rate,  $k_2$ , is proportional to the dislocation velocity and found to be  $k_2 = a \exp(-\frac{E_a}{kT})$ , where  $E_a$  is the activation energy for dislocation motion ( $\sim 1$  eV),  $k$  is the Boltzmann constant, and  $T$  is the temperature in Kelvin, and  $a$  is a pre-exponential factor. A more detailed explanation on this model is

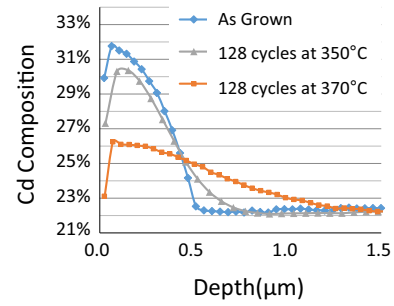


Fig. 7. SIMS showing as grown material and the influence of TCA at two different temperatures.

given in Ref. 12. The modeling results are compared with the experimental results of this work in Fig. 5. There is a reasonable agreement between the experimental results and the model for defect reduction even at the low annealing temperature of 350°C.

The Cd SIMS depth profiles on the samples before and after 128-cycle TCA are shown in Fig. 7. As stated before, the surface layer was grown as a Cd-rich layer with a typical composition of  $x = 0.32$ . The results show that the in-diffusion of Cd from the surface to the MCT bulk is very sensitive to the annealing temperature. The diffusion is minimal for annealing at 350°C. The use of an annealing temperature of only 20°C higher, at 370°C, shows a significantly higher degree of diffusion due to the diffusion coefficient increasing by an order of magnitude from 350°C to 370°C.<sup>16</sup> Therefore, we can minimize dislocation density while maintaining a relatively sharp device structure interface integrity even at annealing temperatures as low as 350°C. As described above, we compensated for the decrease in annealing temperature by increasing the number of anneal cycles to achieve the same minimum EPD density of  $1 \times 10^6 \text{ cm}^{-2}$ .

In this study, we found a significant reduction in EPD with the number of cycles in some samples, while others show very little variation in EPD with TCA. Understanding these differences is necessary for applying the results of this work to the device processing. There are several factors that can limit the utility of TCA. The device structure, initial (as-grown) EPD count of the material, and the thickness of the MCT layer seem to be some of those limiting the final EPD of the annealed samples.

To determine the influence of MCT layer thickness, we performed TCA on MCT layers that are 4  $\mu\text{m}$  thick, which is lower than the 10  $\mu\text{m}$  thickness of the rest of the samples in this work. As shown in Fig. 8, the TCA did not reduce the dislocation density in a 4- $\mu\text{m}$ -thick MCT layer, whereas in MCT layers that are thicker ( $\sim 10 \mu\text{m}$ ), there is a reduced dislocation density, as expected by the model. Previously published depth-based EPD measurements by Farrell et al.<sup>17</sup> for 4-cycle TCA at 494°C showed a reduction in defect density near the surface of the

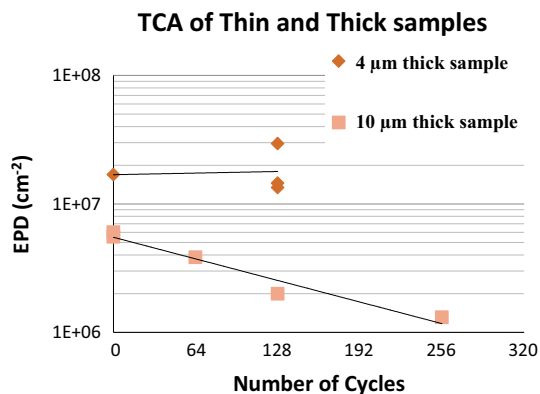


Fig. 8. EPD versus number of cycles comparing thin and thick samples.

sample, but not away from the surface. The defect density began increasing (from the TCA reduced value) with increasing depth from the MCT surface. This increase started at the location which is 5 μm from the MCT/CdTe interface. At the location which is 4 μm from the MCT/CdTe interface, the EPD was ~1 × 10<sup>7</sup> cm<sup>-2</sup>. This means that there is no reduction in defect density at distances less than 4 μm from the MCT/CdTe interface. This indicates that the benefits of TCA can be realized only in samples much thicker than 4 μm. The lattice mismatch-related strain closer to the MCT/CdTe interface is believed to be responsible for this behavior.

To study the applicability of TCA to varied device structures, some samples were designed with varying Cd composition cap layers. One such sample has a high cadmium composition layer at the surface of the MCT layer, as shown in Fig. 9a. The structure of the sample and the annealing results are shown in Fig. 9b. In the sister samples, the high Cd composition layer was removed by a bromine-methanol (0.1%) etch. This experiment was designed to study the limiting nature of having a high stress interface on dislocation density. In our depth-based measurements, we observed an increase in EPD when nearing the Hg<sub>0.5</sub>Cd<sub>0.5</sub>Te/Hg<sub>0.7</sub>Cd<sub>0.3</sub>Te interface and decreasing EPD as we move away from this interface, as seen in Fig. 9. When the anneals were performed after removing the surface layer, the EPD of the sample reduced as is normally expected. This presents a potential issue with the applicability of TCA to complex device structures. Overcoming this problem may require different TCA schedules.

The TCA improves material quality depending on the MCT layer thickness, but we wanted to find out how bad the initial (as-grown) MCT sample quality could be to improve the crystalline quality by TCA. Increasing sample yield is important in industrial applications. If a sample is grown with a high defect density, but can be salvaged by the TCA defect reduction, we can improve the yield of the manufacturing process. Poor growth conditions lead to a

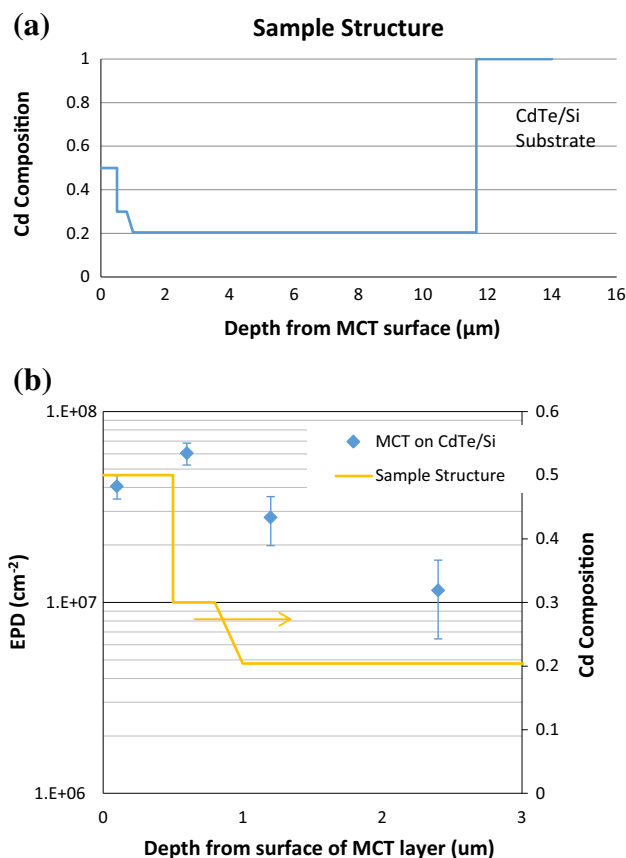


Fig. 9. Structure of sample with (a) the full layer structure from the substrate and (b) EPD versus depth showing the impact of interfaces.

dislocation density of greater than 5 × 10<sup>7</sup> cm<sup>-2</sup>. We conducted several anneals with several different samples that had high EPD. In our study, samples with a high initial EPD showed no improvement with any TCA schedule, even at high anneal temperatures of 500°C.

One of the major problems we initially encountered in the graphite tube TCA setup is mercury condensation on the sample surface. The original ampoule design placed the mercury at the end of the ampoule with the samples sitting on a quartz sample holder. This setup is seen in the schematic in Fig. 10. This caused the mercury to heat faster than the samples and to condense on the surface of the colder MCT samples. By designing a new sample holder in the current annealing setup, we were able to minimize mercury condensation onto the MCT sample surface. In our new design, the mercury is placed in a bowl-shaped container integrated within the quartz sample holder but away from the samples. This structure significantly reduced the condensation of mercury on the sample surface, as can be seen in Fig. 11, because the heating rate is roughly the same for both the mercury and the samples.



Fig. 10. Original ampoule design with mercury placed at the end of the ampoule and samples placed on a carrier.

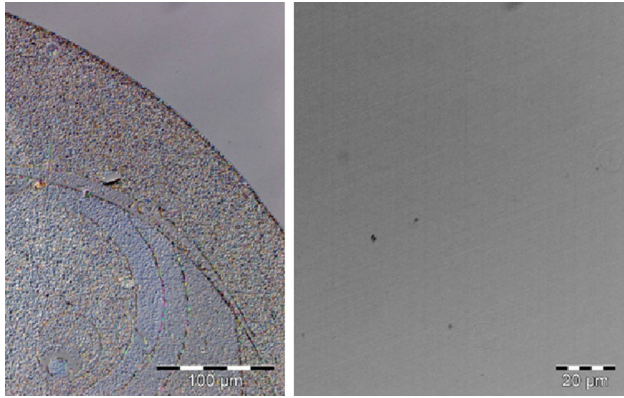


Fig. 11. Sample surface morphology of sample subjected to graphite tube TCA process using the standard ampoule design (left) showing the effect of mercury condensation and (right) using the modified insert design which results in more repeatable low to no mercury condensation on the surface of the samples.

Although the EPD is reduced significantly by the TCA, the main limitation remains the inability to decrease the defect densities below  $1 \times 10^6 \text{ cm}^{-2}$ . This seems to be an inherent limitation to MCT grown on silicon-based substrates. This dislocation density reduction limitation can be problematic for long-wavelength infrared, narrow band-gap devices and requires further study on TCA or alternate annealing methods to achieve EPD of the same order as on the MCT grown on lattice-matched CdZnTe substrates.

## CONCLUSION

We have been able to reduce the dislocation density in samples of MCT grown on CdTe/Si to low  $10^6 \text{ cm}^{-2}$  while minimizing Cd diffusion. Our new TCA setup has allowed faster heating and cooling rates to optimize defect reduction at lower temperatures and also resulted in a better sample surface morphology. We have observed desirable results for an anneal temperature as low as  $350^\circ\text{C}$  and anneal cycle duration of less than 1 min, which significantly limits Cd diffusion while obtaining a lower EPD. We have shown that the EPD does not reduce significantly in the absorber layer of the MCT structure when there is a sharp interface or when the MCT layer is relatively thin ( $< 5 \mu\text{m}$ ). Therefore, dislocation reduction is maximized with minimal

diffusion in samples of thickness greater than  $4 \mu\text{m}$  with TCA at  $350^\circ\text{C}$  for 128 cycles. The main limitation of TCA remains to be the inability to reduce defect density below  $1 \times 10^6 \text{ cm}^{-2}$  for MCT grown on silicon-based substrates. Further work is required for solving this minimum defect density problem.

## ACKNOWLEDGEMENT

The authors would like to thank Defense Advanced Research Projects Agency (DARPA) for funding through Army Research Office (ARO) contract #W911NF-11-2-0049.

## REFERENCES

1. W.D. Lawson, S. Nielsen, E. Putley, and A. Young, *J. Phys. Chem. Solids* 9, 325 (1959).
2. G. Brill, Y. Chen, P. Wijewarnasuriya, and N. Dhar, in *SPIE Infrared Systems and Photoelectric Technology IV*, Adelphi, MD, 2009.
3. S.-W. Sun, C.-H. Zhou, H.-X. Yu, C. Xu, F.-F. Sheng, S.-Y. Sui, J.-R. Yang, and L. He, in *Proceedings SPIE: ISPDI 2013*, Beijing, 2013.
4. J. Benson, L. Bubulac, P. Smith, R. Jacobs, J. Markunas, M. Jaime-Vasquez, L. Almeida, A. Stoltz, J. Arias, G. Brill, Y. Chen, P. Wijewarnasuriya, S. Farrell, and U. Lee, *J. Electron. Mater.* 41, 2971 (2012).
5. M. Carmody, A. Yulius, D. Edwall, D. Lee, E. Piquette, R. Jacobs, D. Benson, A. Stoltz, J. Markunas, A. Almeida, and J. Arias, *J. Electron. Mater.* 41, 2719 (2012).
6. L. Bubulac, J. Benson, R. Jacobs, A. Stoltz, M. Jaime-Vasquez, L. Almeida, A. Wang, L. Wang, R. Hellmer, T. Golding, J. Dinan, M. Carmody, P. Wijewarnasuriya, M. Lee, M. Vilela, J. Peterson, S. Johnson, and D. Lofgreen, *J. Electron. Mater.* 40, 280 (2011).
7. J.-P. Faurie, L.A. Almeida, Y. Chen, R. Sporcken, and S. Sivananthan, in *SPIE Proceedings 2685*, 1996.
8. A. Diaz, S.A. Quinones, and D. Ferrer, *J. Electron. Mater.* 42, 1092 (2013).
9. Y. Chen, S. Farrell, G. Brill, P. Wijewarnasuriya, and N. Dhar, *J. Crystal Growth* 310, 5303 (2008).
10. W. Wang, L. Chen, R. Gu, C. Shen, X. Fu, Y. Guo, G. Wang, F. Yang, and L. He, in *Proceedings SPIE 8419, 6th International Symposium on Advanced Optical Manufacturing and Testing Technologies: Optoelectronic Materials and Devices for Sensing, Imaging, and Solar Energy*, Xiamen, China, 2012.
11. S. Johnson, D. Rhiger, J. Rosbeck, J. Peterson, S. Taylor, and M. Boyd, *J. Vac. Sci. Tech. B* 10, 1499 (1992).
12. J. Benson, S. Farrell, G. Brill, Y. Chen, P. Wijewarnasuriya, L. Bubulac, P. Smith, R. Jacobs, J. Markunas, M. Jaime-Vasquez, L. Almeida, A. Stoltz, U. Lee, M. Vilela, J. Peterson, S. Johnson, D. Lofgreen, and D. Rhiger, 40, 2011.
13. S. Farrell, M. Rao, G. Brill, Y. Chen, P. Wijewarnasuriya, N. Dhar, J. Benson, and K. Harris, *J. Electron. Mater.* 42, 3097 (2013).
14. S. Farrell, G. Brill, Y. Chen, P. Wijewarnasuriya, M.V. Rao, N. Dhar, and K. Harris, *J. Electron. Mater.* 39, 43 (2009).
15. M. Yamaguchi, M. Tachikawa, Y. Itoh, M. Sugo, and S. Kondo, *J. Applied Phys.* 68, 4518 (1990).
16. P. Capper, J. Garland, S. Kasap, and A. Willoughby, *Mercury Cadmium Telluride: Growth, Properties and Applications*, Wiley Series in Materials for Electronic & Optoelectronic Applications, 2010.
17. S. Farrell, M.V. Rao, G. Brill, Y. Chen, P. Wijewarnasuriya, N. Dhar, D. Benson, and K. Harris, *J. Electron. Mater.* 40, 1727 (2011).